Surface Properties of Reverse Osmosis Membrane

Yongyi Yao,[1,2] Shiwei Guo,[2] Yunxiang Zhang[1]

[1]*Chemical Engineering College, Sichuan University, Chengdu 610065, Sichuan, People's Republic of China*
[2]*Postdoctoral Research Studying Station, Guizhou Hongfu Industry and Commerce Development Co. Ltd., Fuquan 550501, Guizhou, People's Republic of China*

Received 18 September 2006; accepted 2 October 2006
DOI 10.1002/app.25656
Published online 16 April 2007 in Wiley InterScience (www.interscience.wiley.com).

ABSTRACT: The morphology and structure of the top surfaces of three commercially Reverse osmosis (RO) membranes (Vontron Eviro-Tech) have been studied using SEM and AFM techniques. As a result, the unevenness of the surface of ULP21 membrane was the greatest and that of SW21 membrane was smooth. The more the roughness of the top surface of the RO membranes was, the larger the flux of the RO membranes was. Accordingly, the roughness of the top surface of RO membranes intensively affected on the performance of RO membrane. © 2007 Wiley Periodicals, Inc. J Appl Polym Sci 105: 1261–1266, 2007

Key words: RO membrane; top surface morphology; roughness

INTRODUCTION

Reverse osmosis (RO) process has widely been applying in many fields for a practical separation such as the desalination of sea water and brackish water, the separation of biochemical process and the treatment of waste water. The RO membrane plays an important role in the separation processes. This membrane allows one of the components (solvent) to pass through and prevents the other (solute) totally or partially from penetrating. This process depends on the physical and chemical properties of the membrane.[1] In these properties of the membrane, the physical properties have great effect on membrane performance. Surface morphology and its roughness are special important in the physical properties of membrane. Numerous RO membranes have been investigated on the surface properties of membrane. Matsuura[2] reviewed the characteristic methods of RO membranes. It is needless to say that SEM has been a powerful tool to investigate the morphology of the top surface of RO membranes. Atomic force microscopy became popular in nineties and many ATM pictures of RO membrane surfaces have been taken.[3–12] Hirose et al.[13] used SEM and AFM surface analytical techniques to investigate the relationship between the surface structures of skin layers of crosslinked aromatic polyamide composite RO membranes and their RO performances. As a result, it was found that RO membranes with rough skin layer surface structures produce high fluxes, and there exists an approximately linear relationship between this surface roughness and RO membrane flux. Stamatialis et al.[14] investigated the surface structure of dense and integrally skinned cellulose acetate and cellulose acetate butyrate membranes by using tapping mode AFM. It was observed that the surface morphology is associated with permeation properties, the lower the value of roughness the lower the flux and the higher the rejection but the relationship was not found to be linear. Kwak and Ihm[15] used AFM, the FE-SEM (field emission-scanning electron microscope) and solid state H nuclear magnetic resonance (NMR) spectroscopy to study the performances of four commercially available aromatic polyamide composite RO membranes. The results showed that the membrane performance depends primarily on the nature of the thin film layer. The roughest membrane has the highest flux. However, a linear relationship between membrane surface roughness and flux was not found. Madaeni[16] showed that the rougher the membrane the lower the permeation rate because of the adsorption and trapping of the ions on the rough surface membrane. His finding is based on evaluating two commercial RO membranes performance in tap water. Based on a thorough review of the literatures for this study, the effect of surface roughness on RO membrane flux is not yet clear and more work in this area needs to be done to understand any potential links between surface roughness and membrane performance.

Correspondence to: Y. Y. Yao (yyyao@tom.com).
Contract grant sponsor: Guizhou Hongfu Industry and Commerce Development Co. Ltd.; contract grant number: 05-2-02-04-03.
Contract grant sponsor: Economic and Trade Commission of Guizhou Province, People's Republic of China; contract grant number: 06031.

In this article, the surface characteristics of commercial available aromatic polyamide composite RO membranes produced by Vontron Enviro-Tech, Ltd. (Guiyang, People's Republic of China), which can operate in ultra-low pressure, low pressure or high pressure, has been studied using scanning electron microscopy (SEM) and atomic force microscopy (AFM). The effect of surface roughness on the membrane performance has been investigated.

EXPERIMENTAL

Three commercially available RO membranes, ULP21, LP21, and SW21, from Vontron Enviro-Tech, (in People's Republic of China), were used in present study.

All average permeate flow (F_w) and salt rejection (R) of the RO membranes were measured by conducting at difference pressures using the NaCl solution concentration in a range of 2000–32,000 ppm at 25°C in cross-flow module.

The average salt rejection was calculated by

$$R = \left(1 - \frac{C_P}{C_f}\right) \times 100 \quad (1)$$

where C_f and C_P are the concentration of NaCl in the bulk of the feed solution and in the permeate solution, respectively.

The average permeate flow is described as

$$F_w = A(\Delta p - \Delta\pi) \quad (2)$$

where A is the coefficient of the permeate flow, L/m^2 h Mpa; Δp is the difference of the pressures crossing the membrane, MPa; $\Delta\pi$ is the difference of permeation pressure crossing the membrane, MPa.

In the permeation experiments, the membrane modules with the efficient area of 7.9 m^2 were used. The permeate solution was collected in 30 min. The initial feed concentration of NaCl solution for ULP21 and LP21 was 2000 mg/L and for SW21 was 35,000 mg/L. The concentrations at the feed and the permeate were determined by conductivity, at 25°C, using a Mettler-Toledo conductimeter (model SG3).

The functional group composition of the membrane surfaces was measured by attenuated total reflection-Fourier transform infrared (ATR–FT–IR) spectroscopy. The spectra were recorded on a spectrometer (FTS3000, Digilab LLC.). All spectra were recorded at 25°C. The instrument was purged with dry nitrogen to prevent interference of atmospheric moisture with the spectra.

To characterize the morphology of the membrane surface, scanning electron microscope (SEM) and atomic force microscope (AFM) were employed.

TABLE I
Average Salt Rejection Rate and Average Permeate Flows for These Three Membranes

Sample	Average salt rejection rate (%)	Average permeate flow (L/m^2 h)	Testing pressure (MPa)
ULP21(B)	99.0	50.1	1.03
LP21(A)	99.5	48.0	1.55
SW21(C)	99.5	25.3	5.50

For SEM the surfaces of the membrane samples were gilded in thickness of 2–3 nm using the EIKO IB-3 ion coater (EIKO Engineering, Japan). The SEM microphotographs were taken by JSM-5900LV (JEOL, Japan).

The AFM (SPA400, Seiko Instruments, Japan) was used in the surface analysis by the dynamic force mode. The surface area of the images was scanned 5×5 μm^2. The surfaces of various membranes are compared in terms of the roughness parameter. The roughness parameters obtained from the AFM images should be considered as the relative roughness value. The same tip was used for all experiments and all captured surfaces were treated in the same way. All AFM images were undertaken at 25°C.

Differences in the membrane surface morphology can be expressed in terms of various roughness parameters which describe as:[11,13]

1. The difference between the highest and the lowest points within the given area, z.
2. The mean roughness (R_a). This parameter represents the mean value of the surface relative to the center plane, the plane for which the volumes enclosed by the image above and below this plane are equal. It is calculated as

$$R_a = \frac{1}{L_x L_y} \int_0^{L_x} \int_0^{L_y} |f(x,y)|\, dxdy \quad (3)$$

   where $f(x,y)$ is the surface relative to the center plane and L_x and L_y. L_y are the dimensions of the surface in the x and y directions, respectively.
3. The square mean roughness (R_{MS}) is represented as

$$R_{MS} = \frac{1}{L_x L_y} \int_0^{L_x} \int_0^{L_y} |f(x,y)|^2\, dxdy \quad (4)$$

4. The maximum difference of peak and valley (P–V) is represented as a difference of a height of maximum peak and a depth of minimum valley in a specific plane.

$$P - V = z_{\max} - z_{\min} \quad (5)$$

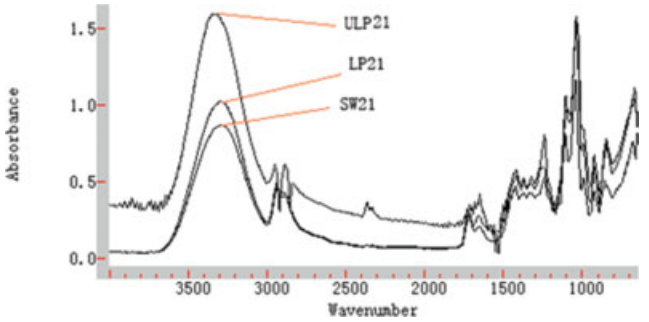

Figure 1 ATR-FTIR spectra of the top surfaces of the membranes. [Color figure can be viewed in the online issue, which is available at www.interscience.wiley.com.]

where z_{max} and z_{min} are a height of maximum peak and a depth of minimum valley in a specific plane, respectively.

5. Ten points mean plane roughness (R_z) is defined in SPA400 for a measurement plane and represented as a difference of a mean of five highest peaks and a mean of five deepest valleys.

All the surface roughness parameters are calculated from the AFM images using an AFM software program (SPI3800 Analysis).

RESULTS AND DISCUSSION

Performance of membranes

Average salt rejection rate and average permeate flows for the three membranes are showed in Table I. For these membranes, the average salt rejection rates are in a range of 99.0–99.5% and the average permeates flows vary from 50.1–25.3 L/m^2 h. The testing Pressure of the sample SW21 is as high as 5.50 MPa. For membrane ULP21, it has the lowest average salt rejection rate (99.0%) and the highest average permeate (50.1 L/m^2 h), this might be determined by its surface structure. From Figure 2(a), the top surface of ULP21 membrane is rather rough. This implied the apertures of the membrane were relatively larger. So the average salt rejection rate was relatively lower. On the other hand, from Figure 2(b), the thickness of surface layer of ULP21 is very thick. This was in favor of passing the liquid through the membrane. For SW21 membrane, the top surface is smooth and compact. This made it have high salt rejection (99.5%). However, because of its compactness and high thickness, the membrane resistance to the passing liquid was very high. To complete this process, the high energy (5.50 MPa) is supplied.

ATR-FTIR of membranes

In Figure 1, ATR–FTIR spectra were recorded in two regions: 4000–2800 cm^{-1}, where the characteristic bands of OH, the NH and CH are to be found, and 1800–1100 cm^{-1}, where the absorption characteristic of the amide group is located. As a result, the materials of the skin layer of ULP21, LP21, and SW21 membranes might be similar. They belong to a kind of the aromatic polyamide.

Characterization of surface structures by SEM

The skin layer structures of three membranes were observed by SEM. The SEM micrograph of the ULP21, LP21, and SW21 membranes skin layers and cross section are shown in Figures 2–4, respectively.

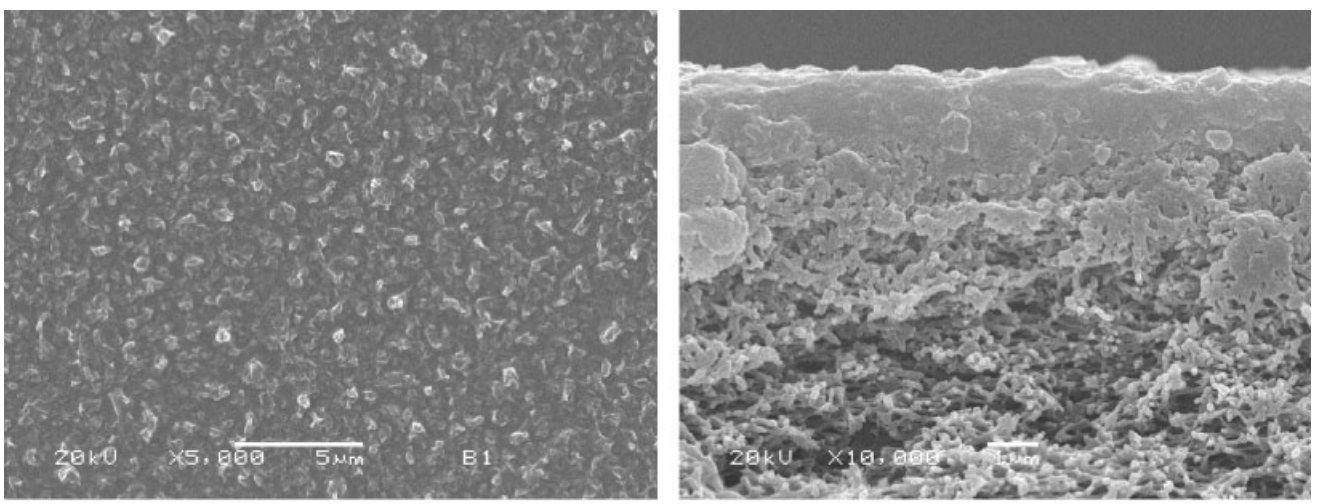

(a) (b)

Figure 2 SEM micrograph of ULP21 membrane skin layers and cross section.

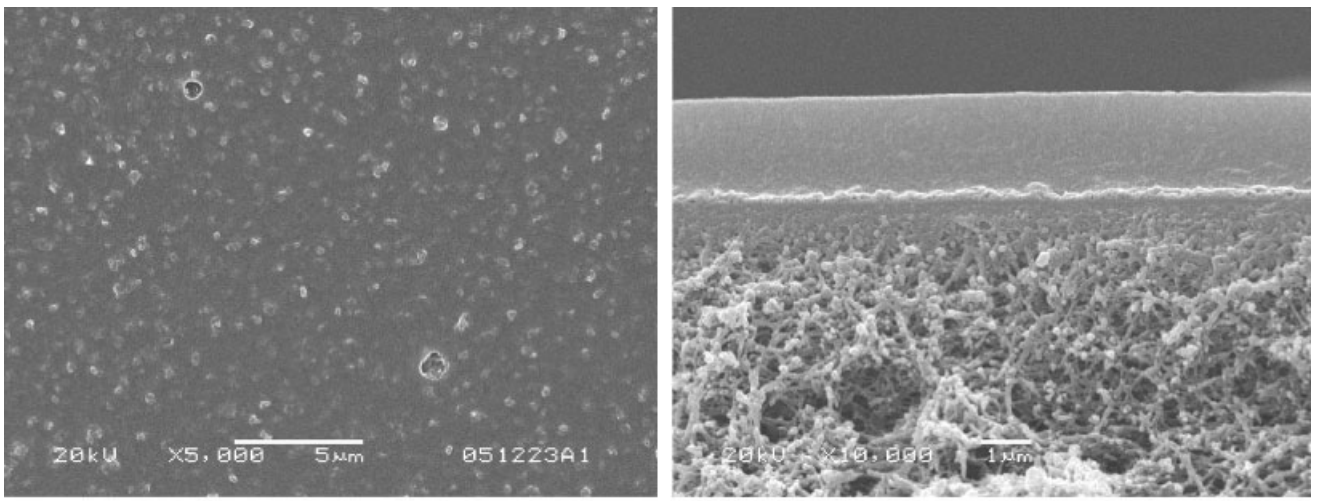

Figure 3 SEM micrograph of LP21 membrane skin layers and cross section.

The top surfaces of the ULP21 and LP21 membranes skin layers shown in Figures 2(a) and 3(a) with three-dimensional structures were not smooth. The magnitude of the unevenness is difference. The magnitude of unevenness of the ULP21 membrane is higher than that of the LP21 membrane. In addition, the smooth surface of the SW membrane could be observed in Figure 4(a). The diversity of the surface of membranes depends on the materials and the preparation methods. Although the materials of three membranes in this investigation are similar, the morphologies of the membranes are unlikeness. It is important that the different preparation method has resulted in completely different surface structure of membranes for the same membrane material. On the other hand, from the SEM micrographs of the cross section of the RO membranes shown in Figures 2(b)–4(b), it is seen that the membranes are divided into three layers including the skin layer, spongy layer and porous layer. The skin layer is the foundational layer and determines the RO performances. The spongy layer provides the sustained structure that could support high pressure. The porous layer allows transporting the permeated solvent. For the skin layer of the RO membranes, three membranes are difference. The thickness of skin

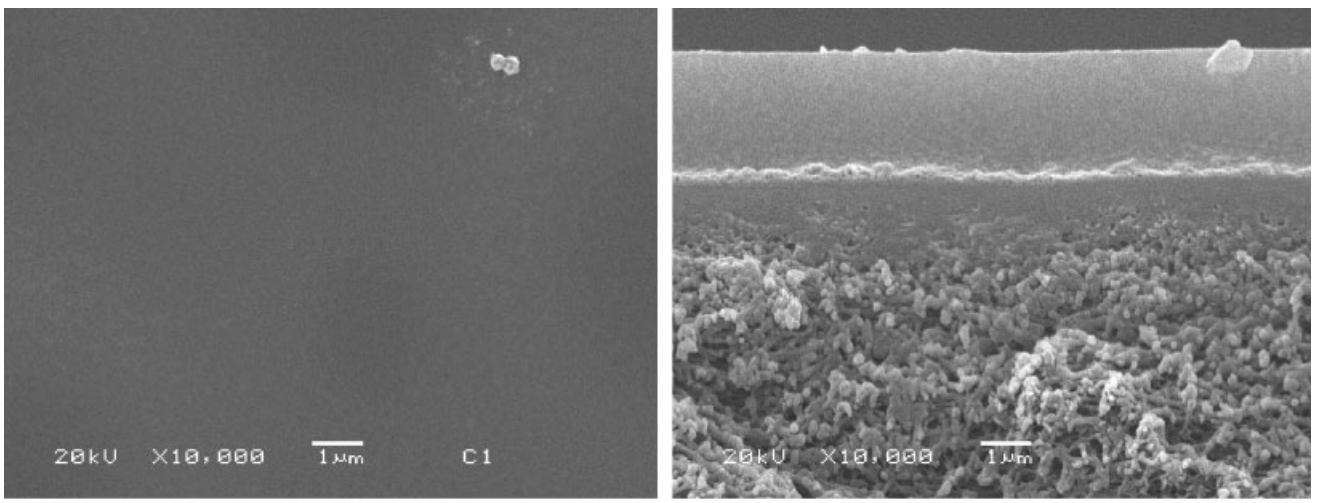

Figure 4 SEM micrograph of SW21 membranes skin layers and cross section.

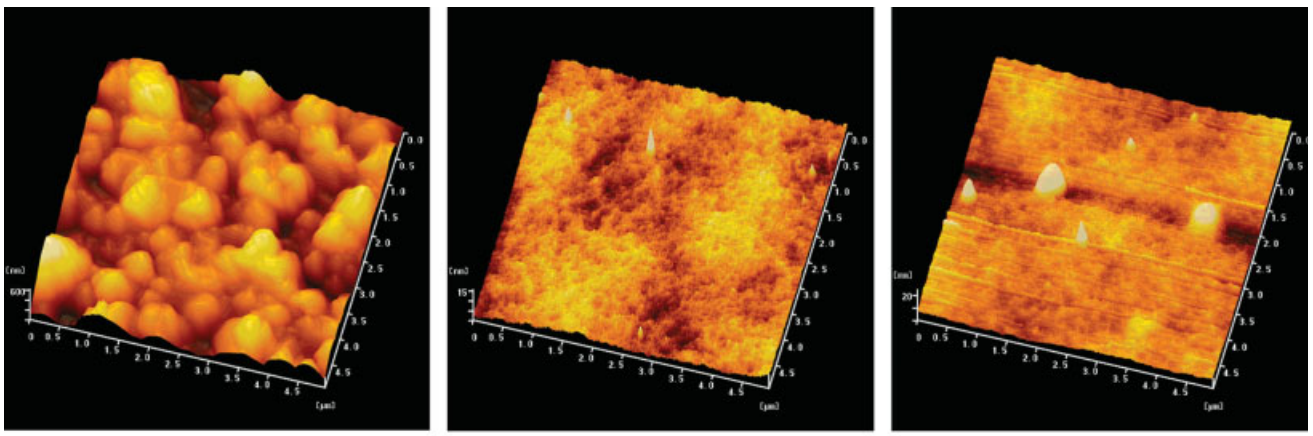

Figure 5 Three-dimension AFM photographs of the top surface of RO membranes. [Color figure can be viewed in the online issue, which is available at www.interscience.wiley.com.]

layer of SW21 membrane is the largest and that of ULP21 membrane is the thickest. From Table I and Figures 2–4, it can be seen that the more uneven the membrane surface had, the larger the flux was.

Characterization of surface structures by AFM

To understand the surface morphology of RO membranes in detail, ATM was employed. Figure 5 showed the three-dimension AFM photographs of the top surface of RO membranes. From Figure 5(a), the surface of ULP21 membrane was very rough. The ULP21 membrane was composed of peaks and valleys. The slight coloration part was the peak and the darker shade part was the valley. On other hand, the other surfaces of LP21 membrane and SW21 membrane are so smooth. In the Figures 5(b,c), there are not apparent to distinguish the peaks and the valleys of skin layers of the membranes. These morphologies still further proved the result of unevenness obtained from the photographs of SEM.

Surface roughness of RO membranes

The AFM photographs of RO membranes could provide the observation of surface roughness of membranes. The values of surface roughness and AFM photographs of each sample were shown in Table II and Figure 6, respectively. The surface roughness values of R_a and R_{MS} of sample ULP21 are 83.3 nm and 1.05×10^2 nm, respectively. These values of the surface roughness are reasonably large. They are $\sim$ 57 times the values of sample LP21 (R_a 1.47 nm and R_{MS} 1.84 nm) and 43 times the values of sample SW21 (R_a 1.81 nm and R_{MS} 2.47 nm). Also, the values R_z and $P - V$ (R_z 347 nm and $P - V$ 654 nm) were $\sim$ 20 times the values (R_z 17.3 nm and $P - V$ 33.5 nm) of the sample LP21 and the values (R_z 20.1 nm and $P - V$ 28.3 nm) of the sample SW21. According to the Table II, on the other hand, it was noted that the surface roughness values of the sample LP21 and SW21 were rather close. These surfaces of membranes are relatively smooth. However, the performances of these membranes were very difference (shown in Table I). The averages permeate flow (48.0 L/m^2 h) of LP21 membrane was about 2 times that (25.3 L/m^2 h) of SW21 membrane. This evidence could be explained as that the skin layer of SW21 membrane is denser than that of LP21 membrane and the thickness of skin layer of SW21 membrane is greater than the values of LP21 membrane.

TABLE II
Surface Roughness Values of RO Skin Layers by AFM

Sample	R_a (nm)	R_{MS} (nm)	R_z (nm)	$P-V$ (nm)
ULP21	83.3	105	347	654
LP21	1.47	1.84	17.3	33.5
SW21	1.81	2.47	20.1	28.3

CONCLUSIONS

The relationship between the morphology and structure of the top surface of RO membranes along with their RO performance has been studied by using SEM and AFM. For the ULP21 membrane, the higher water flux was obtained because of the uneven surface of the membrane. However the surfaces of the LP21 and SW21 membranes were smoother than that of ULP21 membrane. The fluxes of these membranes were relatively lower. As a result, the surface roughness of the RO membrane does effect on the performances of the RO membrane. Accordingly, the further investigation on the

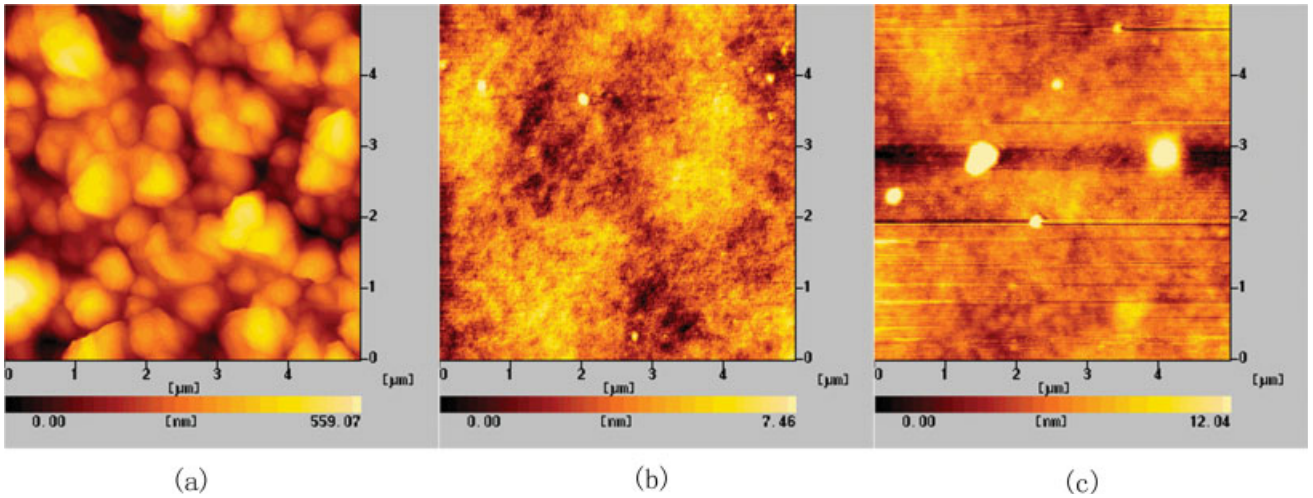

Figure 6 Two-dimension AFM photographs of the top surface of RO membranes. [Color figure can be viewed in the online issue, which is available at www.interscience.wiley.com.]

top surface of RO membranes in future will be needed to understand the effects of the surface structure on the RO performances.

The authors thank Liu Feng (Vontron Enviro-Tech Co., Ltd., Guiyang, People's Republic of China) for providing the samples of RO membranes and thank Mr. Li Zhu and Mr. Tian Yunfei (Research Center For Analysis and Measurement, Sichuan University, Chengdu, People's Republic of China) for their assistance with the SEM and AFM experiments, respectively.

References

1. Madaeni, S. S. J Porous Mater 2004, 11, 255.
2. Matsuura, T. Desalination 2001, 134, 47.
3. Trushinski, B. J.; Dickson, J. M.; Smyth, T.; Childs, R. F.; McCarry, B. E. J Membr Sci 1998, 143, 181.
4. Bowen, W. R.; Doneva, T. A. J Colloid Interface Sci 2000, 229, 544.
5. Bowen, W. R.; Doneva, T. A.; Yin H. B. Desalination 2002, 146, 97.
6. Yoshida, W.; Cohen, Y. J Membr Sci 2003, 215, 249.
7. Khulbe, K. C.; Hamad, F.; Feng, C.; Matsuura, T.; Khayet, M. Desalination 2004, 161, 259.
8. Brant, J. A.; Childress, A. E. J Membr Sci 2004, 241, 235.
9. Hilal, N.; Al-Zoubi, H.; Darwish, N. A.; Mohammad, A. W.; Arabi, M. A. Desalination 2004, 170, 281.
10. Freger, V.; Gilron, J.; Belfer S. J Membr Sci 2002, 209, 283.
11. Bowen, W.; Hilal, N.; Lovitt, R.; Sharif, A.; Williams, P. M. J Membr Sci 1997, 126, 77.
12. Bowen, W.; Hilal, N.; Lovitt, R.; Sharif, A.; Williams, P. M. J Membr Sci 1996, 110, 233.
13. Hirose, M.; Ito, H.; Kamiyama Y. J Membr Sci 1996, 121, 209.
14. Stamatialis, D. F.; Dias, C. R.; Norberta de Pinho, M. J Membr Sci 1999, 160, 235.
15. Kwak, S.-Y.; Ihm, D. W. J Membr Sci 1999, 158, 143.
16. Madaeni, S. S. Desalination 2001, 139, 371.